ARTICLES
PUBLISHED ONLINE: 13 MARCH 2011 | DOI: 10.1038/NPHYS1926
nature physics

Floquet topological insulator in semiconductor quantum wells

Netanel H. Lindner[1,2]*, Gil Refael[1,2] and Victor Galitski[3,4]

Topological phases of matter have captured our imagination over the past few years, with tantalizing properties such as robust edge modes and exotic non-Abelian excitations, and potential applications ranging from semiconductor spintronics to topological quantum computation. Despite recent advancements in the field, our ability to control topological transitions remains limited, and usually requires changing material or structural properties. We show, using Floquet theory, that a topological state can be induced in a semiconductor quantum well, initially in the trivial phase. This can be achieved by irradiation with microwave frequencies, without changing the well structure, closing the gap and crossing the phase transition. We show that the quasi-energy spectrum exhibits a single pair of helical edge states. We discuss the necessary experimental parameters for our proposal. This proposal provides an example and a proof of principle of a new non-equilibrium topological state, the Floquet topological insulator, introduced in this paper.

The discovery of topological insulators in solid-state devices such as HgTe/CdTe quantum wells[1,2], and in materials such as Bi_xSb_{1-x} alloys, Bi_2Te_3 and Bi_2Se_3 (refs 3–5) brings us closer to employing the unique properties of topological phases[6,7] in technological applications[8,9].

Despite this success, the choice of materials that exhibit these unique topological properties remains rather scarce. In most cases we have to rely on serendipity in looking for topological materials in solid-state structures and our means to engineer Hamiltonians and control topological phase transitions are very limited.

Our work demonstrates that new methods to achieve and control topological structures are possible in non-equilibrium conditions, where external time-dependent perturbations represent a rich and versatile resource that can be used to achieve topological spectra in systems that are topologically trivial in equilibrium.

In particular, we show that time-periodic perturbations may give rise to new differential operators with topological insulator spectra, dubbed Floquet topological insulators (FTI), that exhibit chiral edge currents when out of equilibrium and possess other hallmark phenomena associated with topological phases. These ideas, combined with the highly developed technology for controlling low-frequency electromagnetic modes, can enable devices in which fast switching of edge state transport is possible and the spectral properties (velocity) of the edge states can be easily controlled.

The Floquet topological insulators discussed here share many features investigated in previous works. Topological states have been explored from the perspective of quantum walks[10]. Also, a similar philosophy led to proposals for effective magnetic fields[11,12] and spin–orbit coupling[13] in cold-atom systems. A photovoltaic effect has been proposed in graphene[14]. Another insightful analogy is the formation of zero-resistance states in Hall bars at low magnetic fields using radio frequency radiation[15–18]. There is also an article[19] proposing that electric fields with frequencies well below the bandgap can transform the topological phase of the Haldane model[20] into a trivial insulator.

Definition of a Floquet topological insulator

Let us first provide a general construction and definition for a Floquet topological insulator in a generic lattice model, and then discuss a specific realization: a HgTe/CdTe quantum well. The generic many-body Hamiltonian of interest is

$$\check{\mathcal{H}}(t)=\sum_{\mathbf{k}\in \mathrm{BZ}} H_{nm}(\mathbf{k},t)c_{n,\mathbf{k}}{}^{\dagger}c_{m,\mathbf{k}}+\text{h. c.} \qquad (1)$$

where $c_{n,\mathbf{k}}{}^{\dagger}$ and $c_{m,\mathbf{k}}$ are fermion creation/annihilation operators, $\mathbf{k}$ is the momentum defined in the Brillouin zone, and the italic indices, $n,m=1,2,\ldots,N$ label some internal degrees of freedom (for example, spin, sublattice, layer indices, and so on). The $N\times N$ $\mathbf{k}$-dependent matrix $\check{H}(\mathbf{k},t)$ is determined by lattice hoppings and/or external fields, which are periodic in time, $\check{\mathcal{H}}(T+t)=\check{\mathcal{H}}(t)$.

First, we recall that without the time dependence, the topological classification reduces to an analysis of the matrix function, $H(\mathbf{k})$, and is determined by its spectrum[21,22]. An interesting question is whether a topological classification is possible in non-equilibrium situation, that is, when the single-particle Hamiltonian, $\check{H}(\mathbf{k},t)$, in equation (1) does have an explicit time dependence, and whether there are observable physical phenomena associated with this non-trivial topology. Consider the single-particle Schrödinger equation associated with equation (1):

$$[\check{H}(\mathbf{k},t)-i\check{I}\partial_t]\,\Psi_{\mathbf{k}}(t)=0, \quad \text{with } \check{H}(\mathbf{k},t)=\check{H}(\mathbf{k},t+T) \qquad (2)$$

The Bloch–Floquet theory states that the solutions to equation (2) have the form $\Psi_{\mathbf{k}}(t)=\check{S}_{\mathbf{k}}(t)\,\Psi_{\mathbf{k}}(0)$, where the unitary evolution is given by the product of a periodic unitary part and a Floquet exponential

$$\check{S}_{\mathbf{k}}(t)=\check{\mathcal{P}}_{\mathbf{k}}(t)\exp[-i\check{H}_{\mathrm{F}}(\mathbf{k})t], \quad \text{with } \check{\mathcal{P}}_{\mathbf{k}}(t)=\check{\mathcal{P}}_{\mathbf{k}}(t+T) \qquad (3)$$

where $\check{H}_{\mathrm{F}}(\mathbf{k})$ is a self-adjoint time-independent matrix associated with the Floquet operator $\left[\check{H}(\mathbf{k},t)-i\check{I}\partial_t\right]$ acting in the space of periodic functions $\Phi(t)=\Phi(t+T)$, where it leads to a

[1]Institute of Quantum Information, California Institute of Technology, Pasadena, California 91125, USA, [2]Department of Physics, California Institute of Technology, Pasadena, California 91125, USA, [3]Condensed Matter Theory Center, Department of Physics, University of Maryland, College Park, Maryland 20742, USA, [4]Joint Quantum Institute, Department of Physics, University of Maryland, College Park, Maryland 20742, USA. *e-mail: lindner@caltech.edu.

time-independent eigenvalue problem, $[\check{H}(\mathbf{k},t)-i\check{I}\partial_t]\Phi(\mathbf{k},t)=\varepsilon(\mathbf{k})\Phi(\mathbf{k},t)$. The quasi-energies $\varepsilon(\mathbf{k})$ are the eigenvalues of the matrix $\check{H}_{\rm F}(\mathbf{k})$ in equation (3), and in the cases of interest can be divided into separate bands. The full single-particle wavefunction is therefore given by $\Psi(t)=e^{-i\varepsilon t}\Phi(t)$. Note that the quasi-energies are defined modulo the frequency $\omega=2\pi/T$.

The Floquet topological insulator is defined through the topological properties of the time-independent Floquet operator $\check{H}_{\rm F}(\mathbf{k})$, in accordance with the existing topological classification of equilibrium Hamiltonians[21,22].

Most importantly, we show below that the FTI is not only a mathematical concept. We explicitly demonstrate that topological properties can be induced in an otherwise topologically trivial HgTe/CdTe quantum well by using experimentally accessible electromagnetic radiation in the microwave-THz regime.

Topological transition in HgTe/CdTe heterostructures

Below we outline a proposal for the realization of a FTI in zincblende structures such as HgTe/CdTe heterostructures, which are in the trivial phase. These are described by the effective Hamiltonian[1]

$$H(k_x,k_y)=\begin{pmatrix}\check{H}(\mathbf{k}) & 0\\ 0 & \check{H}^*(-\mathbf{k})\end{pmatrix} \tag{4}$$

where

$$\check{H}(\mathbf{k})=\epsilon(\mathbf{k})\check{I}+\mathbf{d}(\mathbf{k})\cdot\check{\boldsymbol{\sigma}} \tag{5}$$

$\mathbf{k}=(k_x,k_y)$ is the two-dimensional wavevector, and $\check{\boldsymbol{\sigma}}=(\check{\sigma}_x,\check{\sigma}_y,\check{\sigma}_z)$ are the Pauli matrices. The vector $\mathbf{d}(\mathbf{k})$ is an effective spin–orbit field. The upper block $\check{H}(\mathbf{k})$ is spanned by states with $m_J=(1/2,3/2)$, whereas the lower block, with $m_J=(-1/2,-3/2)$, is its time-reversed partner.

Let us focus on the upper sub-block. The Hamiltonian (5) has two bands with energies $\epsilon_\pm(\mathbf{k})=\epsilon(\mathbf{k})\pm|\mathbf{d}(\mathbf{k})|$.

The TKNN formula provides the sub-band Chern number[23], which for the Hamiltonian (5) can be expressed as an integer counting the number of times the vector $\hat{\mathbf{d}}(\mathbf{k})$ wraps around the unit sphere as $\mathbf{k}$ wraps around the entire FBZ. In integral form, it is given by

$$C_\pm=\pm\frac{1}{4\pi}\int \mathrm{d}^2\mathbf{k}\,\hat{\mathbf{d}}(\mathbf{k})\cdot[\partial_{k_x}\hat{\mathbf{d}}(\mathbf{k})\times\partial_{k_y}\hat{\mathbf{d}}(\mathbf{k})] \tag{6}$$

where $\hat{\mathbf{d}}(\mathbf{k})=\mathbf{d}(\mathbf{k})/|\mathbf{d}(\mathbf{k})|$ is a unit vector and the $(\pm)$ indices label the two bands.

This elegant mathematical construction also yields important physical consequences, as it is related to the quantized Hall conductance associated with an energy band,

$$\sigma_{xy}=\frac{e^2}{h}C \tag{7}$$

Considering now the full Hamiltonian equation (4), each band is degenerate with its time-reversed partner, which exhibits an opposite Chern number. Although the sum of the Chern numbers for the doubly degenerate band vanishes, their difference does not, and signifies the quantum spin Hall conductance.

Let us return to the upper block of equation (4). Around the Γ point of the first Brillouin zone (FBZ) we can expand the vector $\mathbf{d}(\mathbf{k})$ as[1,24]

$$\mathbf{d}(\mathbf{k})=(Ak_x,Ak_y,M-B\mathbf{k}^2) \tag{8}$$

where the parameters $A<0, B>0$ and M depend on the thickness of the quantum well and on parameters of the materials. We can easily see that the Chern number implied by $\mathbf{d}(\mathbf{k})$ depends crucially on the relative sign of M and B. Within the approximation of equation (8), far away from the Γ point, $\mathbf{d}(\mathbf{k})$ must point south (in the negative z direction). At the Γ point, $\mathbf{d}(\mathbf{k})$ is pointing north for $M>0$, but south for $M<0$. For the simplified band structure, the Chern numbers are clearly $C_\pm=\pm\big[1+\mathrm{sign}(M/B)\big]/2$. For a generic band structure corresponding to equation (8) near the Γ-point, the same logic applies, and we can easily see that a change of sign in M induces a change of the Chern number, C, by 1.

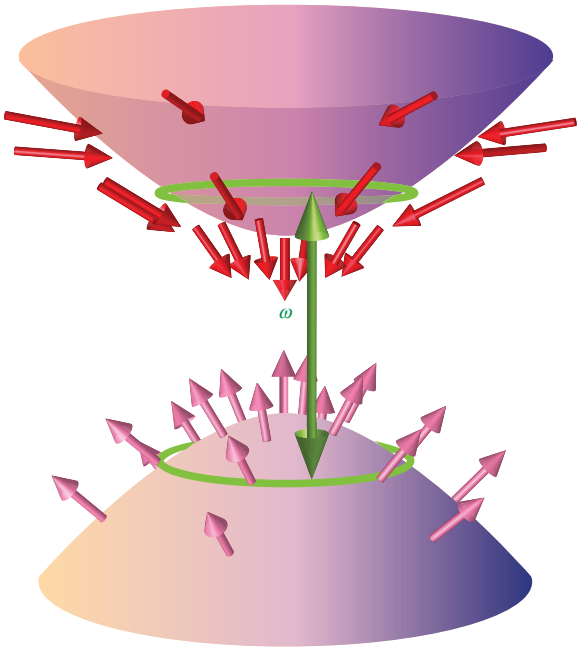

Figure 1 | Inducing an FTI from a trivial insulator. Energy dispersion $\epsilon(\mathbf{k})$ and pseudospin configuration $-\hat{\mathbf{d}}(\mathbf{k})$ for the original bands of $\check{H}(\mathbf{k})$ in the non-topological phase ($M/B<0$). The non-topological phase is characterized by a spin-texture that does not wrap around the unit sphere. On application of a periodic modulation of frequency ω greater than the bandgap, a resonance appears; the green circles and arrow depict the resonance condition.

Starting with the trivial phase ($M<0$), we study periodic modulation of the Hamiltonian, which creates a circle in the FBZ where transitions between the valence and conduction band are at resonance (see Fig. 1). A reshuffled spectrum arises, with new bands consisting of the original ones outside the resonance circle, whereas inside the circle, the original bands are swapped. On the circle, we expect an avoided crossing separating the reshuffled bands. From Fig. 1, we see that this leads to a pseudospin configuration that can potentially have non-trivial topology. Note that the resulting FTI includes contributions from both blocks of equation (4). As we shall show, by tuning the form of the periodic modulation, the FTI could be chosen to be an analog of the quantum spin Hall insulator, protected by an effective time-reversal symmetry, or a quantum Hall insulator where no such symmetry is present.

Floquet topological insulator

Let us next consider the Floquet problem in a zincblende spectrum in detail. We add a time-dependent field to the Hamiltonian (5)

$$\check{V}(t)=\mathbf{V}\cdot\check{\boldsymbol{\sigma}}\cos(\omega t) \tag{9}$$

where $\mathbf{V}$ is a three-dimensional vector that must be carefully chosen to obtain the desired result. It is convenient to transform the bare Hamiltonian to a 'rotating frame of reference' such that

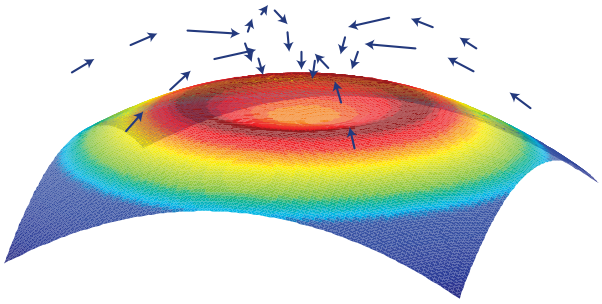

Figure 2 | A topological Floquet band. Pseudospin configuration $\hat{\mathbf{n}}_{\mathbf{k}}$ (blue arrows) and dispersion of the lower band of H_I. Note the dip in the energy surface near $\mathbf{k}=0$, resulting from the reshuffling of the lower and upper bands of $\check{H}(\mathbf{k})$.

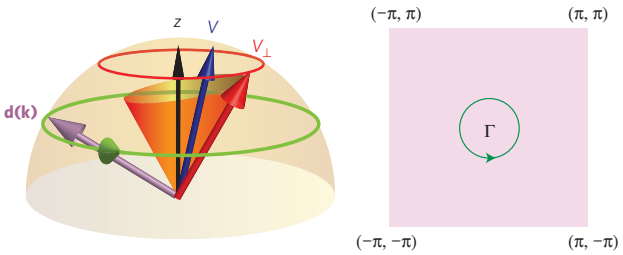

Figure 3 | The geometrical condition for creating topological quasi-energy bands. The purple arrow and green circle depict $\hat{\mathbf{d}}(\mathbf{k})$ on the curve γ in the FBZ (depicted on the right), for which the resonant condition holds. The red arrow and curve depict $\mathbf{V}_\perp(\mathbf{k})$ on γ. The blue arrow depicts the driving field vector $\mathbf{V}$. As long as $\mathbf{V}$ points within the loop traced by $\hat{\mathbf{d}}(\mathbf{k})$, the vector $\mathbf{V}_\perp(\mathbf{k})$ winds around the north pole, which is indicated by the black arrow.

the bottom band is shifted by $\hbar\omega$. This is achieved by using the unitary transformation $\check{U}(\mathbf{k},t)=\check{P}_+(\mathbf{k})+\check{P}_-(\mathbf{k})e^{i\omega t}$, where $\check{P}_\pm(\mathbf{k})=1/2[\check{I}\pm\hat{\mathbf{d}}(\mathbf{k})\cdot\check{\boldsymbol{\sigma}}]$ are projectors on the upper and lower bands of $H(\mathbf{k})$. This results in the following Hamiltonian:

$$\check{H}_I(t)=\check{P}_+(\mathbf{k})\epsilon_+(\mathbf{k})+\check{P}_-(\mathbf{k})[\epsilon_-(\mathbf{k})+\omega]+\check{U}^\dagger\check{V}(t)\check{U} \qquad (10)$$

where $\epsilon_\pm(\mathbf{k})$ are the energies corresponding to $\check{P}_\pm(\mathbf{k})$. In the 'rotating' picture, the two bands cross if ω is larger than the gap M.

H_I is solved by the eigenstates $|\psi_I{}^\pm(\mathbf{k})\rangle$, which for the values of momenta, $\mathbf{k}$, away from the resonance ring are only weakly modified compared to the equilibrium, $\check{V}=0$, case. We define the vector $\hat{\mathbf{n}}_{\mathbf{k}}=\langle\psi_I{}^-(\mathbf{k})|\check{\boldsymbol{\sigma}}|\psi_I{}^-(\mathbf{k})\rangle$, which characterizes the pseudospin configuration in the lower $(-)$ band of H_I (the pseudospin configuration in the upper $(+)$ band points in the opposite direction). The vector $\hat{\mathbf{n}}_{\mathbf{k}}$, which will encode the topological properties of the FTI, is plotted in Fig. 2 for $M/B<0$. Indeed, we see that $\hat{\mathbf{n}}_{\mathbf{k}}$ points towards the south pole near the Γ point, and towards the north pole for larger values of $\mathbf{k}$. These two regimes are separated by the resonance ring, denoted by γ, for which $\omega=\epsilon_+(\mathbf{k})-\epsilon_-(\mathbf{k})$ (the green curve in Fig. 1).

The topological aspects of the reshuffled bands depend crucially on the properties of $\hat{\mathbf{n}}_{\mathbf{k}}$ on γ. These are best illustrated by employing the rotating wave approximation, as we shall proceed to do below. An exact numerical solution, which does not rely on this approximation, will be presented in the next section.

The driving field $\check{V}(t)$ contains both counter-rotating and co-rotating terms. The rotating wave approximation, which is valid under the condition that the detuning, $\Delta=|(\epsilon_+-\epsilon_-)-\omega|$, satisfies $\Delta\ll(\epsilon_+-\epsilon_-)+\omega$, describes correctly the single photon resonance between the conduction and valence bands. In this approximation, counter-rotating terms are omitted and the driving term is given by

$$\check{V}_{\mathrm{RWA}}=\check{P}_+(\mathbf{k})(\mathbf{V}\cdot\check{\boldsymbol{\sigma}})\check{P}_-(\mathbf{k})+\check{P}_-(\mathbf{k})(\mathbf{V}\cdot\check{\boldsymbol{\sigma}})\check{P}_+(\mathbf{k}) \qquad (11)$$

Next, we decompose the vector $\mathbf{V}$ as follows

$$\mathbf{V}=\big(\mathbf{V}\cdot\hat{\mathbf{d}}(\mathbf{k})\big)\hat{\mathbf{d}}(\mathbf{k})+\mathbf{V}_\perp(\mathbf{k}) \qquad (12)$$

A substitution in equation (11) gives

$$\check{V}_{\mathrm{RWA}}=\mathbf{V}_\perp(\mathbf{k})\cdot\check{\boldsymbol{\sigma}} \qquad (13)$$

On the curve γ we have

$$\hat{\mathbf{n}}_{\mathbf{k}}=-\mathbf{V}_\perp(\mathbf{k})/|\mathbf{V}_\perp(\mathbf{k})| \qquad (14)$$

Now, $\mathbf{V}_\perp(\mathbf{k})$ lies on the plane defined by $\hat{\mathbf{d}}(\mathbf{k})$ and $\mathbf{V}$. On the curve γ, $\hat{\mathbf{d}}(\mathbf{k})$ traces a closed loop encircling the north pole on the unit sphere. If this loop encircles the vector $\mathbf{V}$, then $\mathbf{V}_\perp(\mathbf{k})$ will also trace a (different) loop encircling the north pole, as illustrated by Fig. 3.

We can define a topological invariant C^{F} similar to C in equation (6), by replacing $\hat{\mathbf{d}}(\mathbf{k})$ with $\hat{\mathbf{n}}_{\mathbf{k}}$. Under the conditions stated above and with $M<0$, the vector field $\hat{\mathbf{n}}_{\mathbf{k}}$ starts from the south pole at the Γ point and continues smoothly to the northern hemisphere for larger values of $|\mathbf{k}|$ while winding around the equator. For values of $\mathbf{k}$ further away from the curve γ, $\hat{\mathbf{n}}_{\mathbf{k}}\approx-\hat{\mathbf{d}}(\mathbf{k})$, as the driving field is off resonance there. The contribution of these $\mathbf{k}$s to C^{F} is therefore equal to their contribution to C. Therefore it is evident that $C_\pm{}^{\mathrm{F}}=C_\pm\pm1$. Note that for $M>0$, $C_\pm{}^{\mathrm{F}}=C_\pm\mp1$.

A comment is in order regarding the time dependence of C^{F}. As the solutions to the time-dependent Schrödinger equation are given by the transformation,

$$|\psi^\pm(t,\mathbf{k})\rangle=U(t)|\psi_I^\pm(\mathbf{k})\rangle \qquad (15)$$

the pseudospin configuration in the Brillouin zone of these solutions,

$$\hat{\mathbf{n}}_{\mathbf{k}}(t)=\langle\psi^-(\mathbf{k},t)|\check{\boldsymbol{\sigma}}|\psi^-(\mathbf{k},t)\rangle \qquad (16)$$

will also depend on time. However, as we show below, both $\hat{\mathbf{n}}_{\mathbf{k}}$ and $\hat{\mathbf{n}}_{\mathbf{k}}(t)$ (at any time) give the same, time-independent C^{F}. Indeed, the fact that H_I is non-degenerate, implies that both $\hat{\mathbf{n}}_{\mathbf{k}}$ and $\hat{\mathbf{n}}_{\mathbf{k}}(t)$ are well defined in the FBZ. Therefore, C^{F}, as calculated by either of them is a topological invariant that is quantized to an integer and is robust to smooth variations of these vector fields. The two vector fields $\hat{\mathbf{n}}_{\mathbf{k}}$, $\hat{\mathbf{n}}_{\mathbf{k}}(t)$ coincide at $t=0$ and the time dependence resulting from equation (15) constitutes a smooth deformation of $\hat{\mathbf{n}}_{\mathbf{k}}(t)$. Therefore, they both define the same, time-independent, topological invariant C^{F}.

Non-equilibrium edge states

One of the most striking results of the above considerations is the existence of helical edge states once the time-dependent field is turned on. Below we demonstrate the formation of edge states in a tight binding model that contains the essential features of equation (5). The Fourier transform of the spin–orbit coupling vector, $\mathbf{d}(\mathbf{k})$ in the corresponding lattice model is given by, c.f., equation (8),

$$\mathbf{d}(\mathbf{k})=(A\sin k_x, A\sin k_y, M-4B+2B[\cos k_x+\cos k_y]) \qquad (17)$$

We consider the above model with the time-dependent field of the form $V_0\check{\sigma}_z\cos(\omega t)$ in the strip geometry, with periodic boundary condition in the x direction, and vanishing boundary conditions at $y=0,L$.

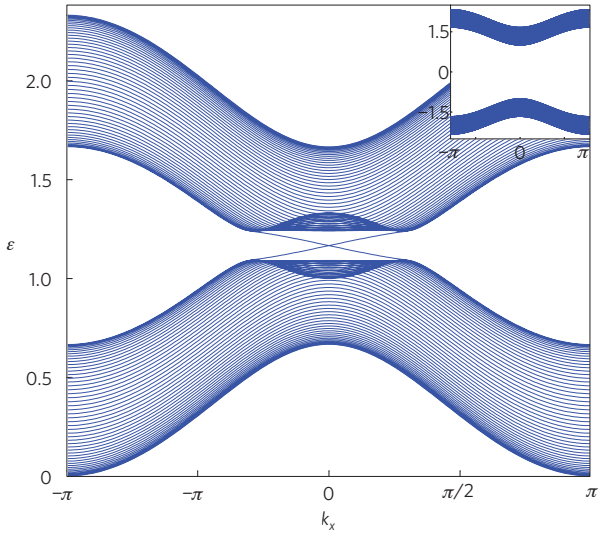

Figure 4 | Edge states in the quasi-energy spectrum. Quasi-energy spectrum of the Floquet equation (3) of the Hamiltonian (17), in the strip geometry: periodic boundary conditions in the x direction, and vanishing ones in the y direction. The driving field was taken to be in the $\hat{\mathbf{z}}$ direction. The horizontal axis labels the momentum k_x. The vertical axis labels the quasi-energies in units of $|M|$. Two linearly dispersing chiral edge modes traverse the gap in the quasi-energy spectrum. The parameters used are $\omega = 2.3|M|$, $|\mathbf{V}| = A = |B| = 0.2|M|$. The inset shows the dispersion of the original Hamiltonian (17), for the same parameters.

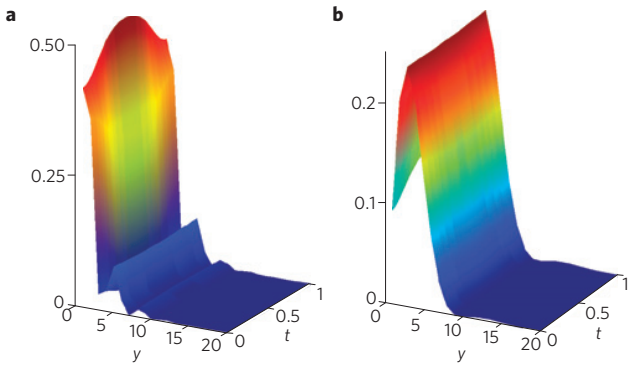

Figure 5 | Time dependence of the edge states. Density of edge mode as function of time, $|\phi(y,t)|^2$, **a** for $k_x = 0$, and **b** for $k_x = 0.84$, where the edge modes meet the bulk states. The horizontal axis shows the distance from the edge, y, in units of the lattice constant, and the time in units of $2\pi/\omega$. For clarity the density for only the 20 lattice sites closest to the edge are shown.

We solve the Floquet equation numerically by moving to frequency space and truncating the number of harmonics. The wavevector k_x is therefore a good quantum number, and the solutions $\Phi(t)$ are characterized by ε and k_x. The quasi-energies for this geometry are shown in Fig. 4. The quasi-energies of the bottom and top bands represent modes that are extended spatially, whereas for each value of k_x there are two modes that are localized in the y direction.

As is evident from Fig. 4, the quasi-energies of these modes disperse linearly, $\varepsilon(k_x) \propto k_x$, hence they propagate with a fixed velocity. Consider a wave packet that is initially described by $f_0(k_x)$. From equation (3) we see that it will evolve into $\psi(t) = \int \mathrm{d}k_x e^{i\varepsilon(k_x)t} f_0(k_x) \Phi^e_{k_x}(y,t)$, where $\Phi^e_{k_x}$ denotes the quasi-energy edge states with momentum k_x. Clearly, this will give a velocity of $\langle \dot{x} \rangle = \int \mathrm{d}k_x |f(k_x)|^2 (\partial\varepsilon/\partial k_x)$.

In general, the solutions $\Phi_{\varepsilon,k_x}(t)$ are time-dependent. An important finding is that the density of the edge modes are only very weakly dependent on time. This can be seen in Fig. 5, in which we plot the time dependence of the density profile of these modes.

Experimental realization of the FTI

To experimentally realize the proposed state, we need to identify a proper time-dependent interaction in the HgTe/CdTe wells. Below we consider several options, of which the most promising uses a circularly polarized electric field.

Magnetic field realization. Perhaps the simplest realization of a time-dependent perturbation of the form (9) is by a microwave-THz oscillating magnetic field, polarized in the $\hat{\mathbf{z}}$ direction. The effect of Zeeman energies in thin Hg/CdTe quantum wells can be evaluated by recalling that the effective model (4) includes states with $m_J = \pm(1/2, 3/2)$ in the upper and lower block respectively. This would result in an effective Zeeman splitting between the two states in each block[24]. The value for the g-factor for HgTe semiconductor quantum wells was measured to be $g \approx 20$ (ref. 25). Therefore, a gap in the quasi-energy spectrum on the order of 0.1 K can be achieved using magnetic fields of 10 mT. Larger gaps may be achieved by using Se instead of Te, as its g-factor is roughly twice as large[26].

As can be seen by inspecting equation (12), the Chern numbers C^{F} for each block in this realization depend only on the winding of the vector $\hat{\mathbf{d}}(\mathbf{k})$. Therefore, the two blocks will exhibit opposite C^{F}, resulting in two counter-propagating helical edge modes. As we explain in the next section, the counter-propagating edge modes cannot couple to open a gap in the quasi-energy spectrum, even though a magnetic field is odd under time reversal.

Stress modulation. Stress modulation of the quantum wells using piezo-electric materials would lead to modulation of the parameter M in (5) and to two counter-propagating edge states.

Electric field realization. An in-plane electric field can produce large gaps in the quasi-energy spectrum and lead to robust co-propagating edge modes. The electric field is given by

$$\check{E} = \mathrm{Re}\,(\boldsymbol{\mathcal{E}} \cdot \exp i\omega t)\, i\nabla_{\mathbf{k}} \tag{18}$$

Inserting this into equation (11), we get

$$\mathbf{V}_\perp(\mathbf{k}) = \hat{\mathbf{d}}(\mathbf{k}) \times (\mathrm{Re}\,\boldsymbol{\mathcal{E}} \cdot \nabla_{\mathbf{k}})\hat{\mathbf{d}}(\mathbf{k}) - (\mathrm{Im}\,\boldsymbol{\mathcal{E}} \cdot \nabla_{\mathbf{k}})\hat{\mathbf{d}}(\mathbf{k}) \tag{19}$$

As before, the vector field $\mathbf{V}_\perp(\mathbf{k})$ is orthogonal to $\hat{\mathbf{d}}(\mathbf{k})$, and again, we would like it to wind around the north pole. Now if we take $\boldsymbol{\mathcal{E}} = \mathcal{E}(-i\hat{\mathbf{x}} - \hat{\mathbf{y}})$ we get, expanding equation (19) to second order in k_x, k_y,

$$\mathbf{V}_\perp(\mathbf{k}) = \frac{A(A^2 - 4BM)\mathcal{E}}{M^3}\left[\frac{1}{2}({k_x}^2 - {k_y}^2)\hat{\mathbf{x}} + k_x k_y \hat{\mathbf{y}}\right] \tag{20}$$

Evidently, the vector field $\mathbf{V}_\perp(\mathbf{k})$ winds twice around the equator. Therefore, for the above choice of $\boldsymbol{\mathcal{E}}$, the Chern numbers will be $C_\pm{}^{\mathrm{F}} = \pm 2$ (and $C^{\mathrm{F}} = 0$ for the lower block). Therefore, each edge of the system will have two co-propagating chiral modes, which cannot be gapped out. Naturally, a choice of $\boldsymbol{\mathcal{E}} = \mathcal{E}(-i\hat{\mathbf{x}} + \hat{\mathbf{y}})$ will give $C^{\mathrm{F}}_\pm = \mp 2$ for the lower block and $C^{\mathrm{F}} = 0$ for the upper block. For HgTe/CdTe quantum wells with thickness of 58 Å (ref. 1), we have

$|\mathbf{V}(\mathbf{k})/\mathcal{E}| \approx 0.1$ mm at $|K| \sim 0.1$ Å. Such a resonance leads to a gap in the quasi-energy spectrum on the order of 10 K even for modest electric fields, on the order of 10 V/m, which are experimentally accessible with powers < 1 mW. Decreasing the well thickness increases[27] the value of $|A/M|$, which can help achieve even larger gaps in the quasi-energy spectrum. We note that, in general, multiple photon resonances can open more gaps in the quasi-energy spectrum. However, these effects will be highly suppressed for the illumination intensities and frequencies considered here.

Discussion

In summary, we have shown that the quasi-energy spectrum of an otherwise ordinary band insulator irradiated by electromagnetic fields can exhibit non-trivial topological invariants and chiral edge modes. A realization of these ideas in zincblende systems, such as HgTe/CdTe semiconducting quantum wells, can lead to Floquet topological insulators that support either co- or counter-propagating helical edge modes. The Floquet operators of these realizations belong, respectively, to symmetry classes analogous to classes A (no symmetry) and AII (time-reversal symmetry with $\mathcal{T}^2 = -1$) in ref. 21.

The symmetry class of the Floquet topological insulator indeed requires careful consideration when two counter-propagating edge states are present, as in the oscillating magnetic-field realization suggested in the previous section. In time-independent systems, topological phases exhibiting counter-propagating edges are only distinct from trivial phases under the restriction $\mathcal{T}\check{\mathcal{H}}\mathcal{T}^{-1} = \check{\mathcal{H}}$, where $\mathcal{T}$ is the anti-unitary time-reversal operator satisfying $\mathcal{T}^2 = -1$. In the time-periodic case, the Hamiltonian at any given time may not possess any symmetry under time reversal. Nevertheless, when the condition

$$\mathcal{T}\check{\mathcal{H}}(t)\mathcal{T}^{-1} = \check{\mathcal{H}}(-t+\tau) \tag{21}$$

holds (for some fixed τ), the Floquet matrix of equation (3) satisfies $\tilde{\mathcal{T}}\check{H}_{\mathrm{F}}(\mathbf{k})\tilde{\mathcal{T}}^{-1} = \check{H}_{\mathrm{F}}(-\mathbf{k})$, where $\tilde{\mathcal{T}}$ is an anti-unitary operator that is related to $\mathcal{T}$ by $\tilde{\mathcal{T}} = V^{\dagger}\mathcal{T}V$, with $V = \check{S}_{\mathbf{k}}(-(T+\tau)/2)$, c.f. equation (3). Clearly, $\tilde{\mathcal{T}}^2 = -1$. Therefore, under this condition, the quasi-energy spectrum consists of analogues to Kramer's doublets, which cannot be coupled by the Floquet matrix. The counter-propagating edge-modes are such a Kramer's pair, which, therefore, cannot couple and open a gap (in the quasi-energy spectrum) under any perturbations satisfying equation (21) (see also ref. 28). We note that equation (21) holds for any Hamiltonian of the form $\check{\mathcal{H}}(t) = \check{\mathcal{H}}_0 + \check{V}\cos(\omega t + \phi)$, with time-reversal invariant $\check{\mathcal{H}}_0$, and $\check{V}$ having unique parity under time reversal, that is, $\mathcal{T}\check{V}\mathcal{T}^{-1} = \pm\check{V}$. An oscillating magnetic field, being odd under time reversal, therefore obeys equation (21) and leads to two counter-propagating edge modes.

An important question concerns the onset and steady states[29] of the driven systems. We emphasize that in the presence of time-dependent fields, response functions including Hall conductivity will be determined not only by the spectrum of the Floquet operator, but also by the distribution of electrons on this spectrum. These in turn depend on the specific relaxation mechanisms present in the system, such as electron–phonon mechanisms[30,31] and electron–electron interaction[32,33].

One way to minimize the unwanted non-equilibrium heating effects would be to use an adiabatic build-up of the Floquet topological insulator state, for example, with the frequency of the modulation gradually increasing from zero to a value larger than the bandgap while keeping the amplitude constant. This should result, at least initially, in an adiabatic loading of the Floquet band originating from the valence band. Nevertheless, relaxation mechanisms will always produce mobile bulk quasi-particles. These effects might be suppressed by restricting the corresponding optical modes in the environment. An analysis of the non-equilibrium states of the system will be the subject of future work.

Received 2 September 2010; accepted 14 January 2011; published online 13 March 2011

References

1. Bernevig, B. A., Hughes, T. L. & Zhang, S. C. Quantum spin Hall effect and topological phase transition in HgTe quantum wells. *Science* **314,** 1757–1761 (2006).
2. König, M. Quantum spin Hall insulator state in HgTe quantum wells. *Science* **318,** 766–770 (2007).
3. Hsieh, D. *et al.* A topological Dirac insulator in a quantum spin Hall phase. *Nature* **452,** 970–974 (2008).
4. Xia, Y. *et al.* Observation of a large-gap topological-insulator class with a single Dirac cone on the surface. *Nature Phys.* **5,** 398–402 (2009).
5. Zhang, H. *et al.* Topological insulators in Bi_2Se_3, Bi_2Te_3, Sb_2Te_3 with a single Dirac cone on the surface. *Nature Phys.* **5,** 438–442 (2009).
6. Fu, L. & Kane, C. L. Superconducting proximity effect and Majorana fermions at the surface of a topological insulator. *Phys. Rev. Lett.* **100,** 096407 (2008).
7. Moore, G. & Read, N. Nonabelions in the fractional quantum Hall effect. *Nucl. Phys. B* **360,** 362–396 (1991).
8. Žutić, I., Fabian, J. & Das Sarma, S. Spintronics: Fundamentals and applications. *Rev. Mod. Phys.* **76,** 323–410 (2004).
9. Nayak, C., Simon, S. H., Stern, A., Freedman, M. & Das Sarma, S. Non-Abelian anyons and topological quantum computation. *Rev. Mod. Phys.* **80,** 1083–1159 (2008).
10. Kitagawa, T., Rudner, M. S., Berg, E. & Demler, E. Exploring topological phases with quantum walks. *Phys. Rev. A* **82,** 033429 (2010).
11. Sörensen, A. S., Demler, E. & Lukin, M. D. Fractional quantum Hall states of atoms in optical lattices. *Phys. Rev. Lett.* **94,** 086803 (2005).
12. Lin, Y. J., Compton, R. L., Jimenez-Garcia, K., Porto, J. V. & Spielman, I. B. Synthetic magnetic fields for ultracold neutral atoms. *Nature* **462,** 628–632 (2009).
13. Stanescu, T. D., Galitski, V., Vaishnav, J. Y., Clark, C. W. & Das Sarma, S. Topological insulators and metals in atomic optical lattices. *Phys. Rev. A* **79,** 053639 (2009).
14. Oka, T. & Aoki, H. Photovoltaic Hall effect in graphene. *Phys. Rev. B* **79,** 081406(R) (2009).
15. Mani, R. G. *et al.* Zero-resistance states induced by electromagnetic-wave excitation in GaAs/AlGaAs heterostructures. *Nature* **420,** 646–650 (2002).
16. Zudov, M. A., Du, R. R., Pfeiffer, L. N. & West, K. W. Evidence for a new dissipationless effect in 2D electronic transport. *Phys. Rev. Lett.* **90,** 046807 (2003).
17. Auerbach, A. & Pai, G. V. Nonlinear current of strongly irradiated quantum Hall gas. *Phys. Rev. B* **76,** 205318 (2007).
18. Dmitriev, I. A., Vavilov, M. G., Aleiner, I. L., Mirlin, A. D. & Polyakov, D. G. Theory of microwave-induced oscillations in the magnetoconductivity of a two-dimensional electron gas. *Phys. Rev. B* **71,** 115316 (2005).
19. Inoue, J. & Tanaka, A. Photoinduced transition between conventional and topological insulators in two-dimensional electronic systems. *Phys. Rev. Lett.* **105,** 017401 (2010).
20. Haldane, F. D. M. Model for a quantum Hall effect without Landau levels: Condensed-matter realization of the 'parity anomaly'. *Phys. Rev. Lett.* **61,** 2015–2018 (1988).
21. Schnyder, A. P., Ryu, S., Furusaki, A. & Ludwig, A. W. W. Classification of topological insulators and superconductors in three spatial dimensions. *Phys. Rev. B* **78,** 195125 (2008).
22. Kitaev, A. Periodic table for topological insulators and superconductors. *AIP Conf. Proc.* **1134,** 22–30; (2009) preprint at http://arxiv.org/abs/0901.2686.
23. Thouless, D. J., Kohmoto, M., Nightingale, M. P. & den Nijs, M. Quantized Hall conductance in a two-dimensional periodic potential. *Phys. Rev. Lett.* **49,** 405–408 (1982).
24. Novik, E. G. *et al.* Band structure of semimagnetic $Hg_{1-y}Mn_yTe$ quantum wells. *Phys. Rev. B* **72,** 035321 (2005).
25. Zhang, X. C., Ortner, K., Pfeuffer-Jeschke, A., Becker, C. R. & Landwehr, G. Effective g factor of n-type $HgTe/Hg_{1-x}Cd_xTe$ single quantum wells. *Phys. Rev. B* **69,** 115340 (2004).
26. Willatzen, M., Cardona, M. & Christensen, N. E. Spin–orbit coupling parameters and electron g factor of II–VI zinc-blende materials. *Phys. Rev. B.* **51,** 17992–17994 (1995).
27. Rothe, D. G. *et al.* Fingerprint of different spin–orbit terms for spin transport in HgTe quantum wells. *New J. Phys.* **12,** 065012 (2010).
28. Kitagawa, T., Berg, E., Rudner, M. & Demle, E. Topological characterization of periodically driven quantum systems. *Phys. Rev. B* **82,** 235114 (2010).
29. Robertson, A. & Galitski, V. M. Nonequilibrium enhancement of Cooper pairing in cold fermion systems. *Phys. Rev. A* **80,** 063609 (2009).

30. Eliashberg, G. M. Film superconductivity stimulated by a high-frequency field. *JETP Lett.* **11,** 114–116 (1970).
31. Eliashberg, G. M. in *Nonequilibrium Superconductivity* (eds Langenberg, D. N. & Larkin, A. I.) (North-Holland, 1986).
32. Glazman, L. I. Resonant excitation of carriers in a semiconductor by a high-power laser pulse. *Sov. Phys. JETP* **53,** 178–181 (1981).
33. Glazman, L. I. Kinetics of electrons and holes in direct gap seminconductors photoexcited by high intensity pulses. *Sov. Phys.—Semicond.-USSR* **17,** 494–498 (1983).

Acknowledgements

We thank J. Avron, A. Auerbach, E. Berg, A. Bernevig, J. Eisenstein, L. Fidkowski, V. Gurarie, I. Klich, and A. Polkovnikov for illuminating conversations. This research was supported by DARPA (G.R., V.G.), NSF grants PHY-0456720 and PHY-0803371 (G.R., N.H.L.). N.H.L. acknowledges the financial support of the Rothschild Foundation and the Gordon and Betty Moore Foundation.

Author contributions

N.H.L., G.R. and V.G. contributed to the conceptual developments. N.H.L. carried out the mathematical analysis.

Additional information

The authors declare no competing financial interests. Supplementary information accompanies this paper on www.nature.com/naturephysics. Reprints and permissions information is available online at http://npg.nature.com/reprintsandpermissions. Correspondence and requests for materials should be addressed to N.H.L.